# Nanoscale

Accepted Manuscript


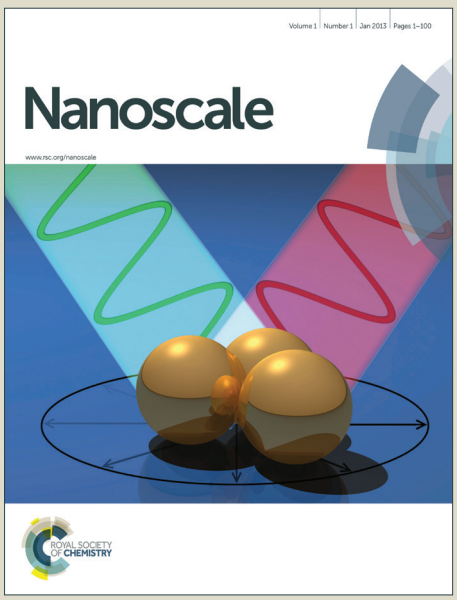





ROYAL SOCIETY OF CHEMISTRY

www.rsc.org/nanoscale

Cite this: DOI: 10.1039/c0xx00000x

www.rsc.org/xxxxxx

ARTICLE TYPE

# Emergence of Metallicity in Silver Clusters in the 150 Atom Regime: A Study of Differently Sized Silver Clusters

**Indranath Chakraborty, Jayanthi Erusappan, Anuradha Govindarajan, K. S. Sugi, Thumu Udayabhaskararao, Atanu Ghosh and Thalappil Pradeep***

***Received (in XXX, XXX) Xth XXXXXXXXX 20XX, Accepted Xth XXXXXXXXX 20XX***
**DOI: 10.1039/b000000x**

We report the systematic appearance of a plasmon-like optical absorption feature in silver clusters protected with 2-phenylethanethiol (PET), 4-flurothiophenol (4-FTP) and (4-(t-butyl)benzenethiol (BBS), as a function of cluster size. A wide range of clusters, namely, $Ag_{44}(4\text{-FTP})_{30}$, $Ag_{55}(PET)_{31}$, ~$Ag_{75}(PET)_{40}$, ~$Ag_{114}(PET)_{46}$, $Ag_{152}(PET)_{60}$, ~$Ag_{202}(BBS)_{70}$, ~$Ag_{423}(PET)_{105}$, and ~$Ag_{530}(PET)_{100}$ were prepared. The UV/Vis spectra show multiple features up to ~$Ag_{114}$ and thereafter from $Ag_{152}$ onwards, the plasmonic feature corresponding to a single peak at ~ 460 nm evolves which points to the emergence of metallicity in clusters composed of ~ 150 metal atoms. A minor blue shift in the plasmonic peak was observed as cluster size increases and merges with the spectrum of plasmonic nanoparticles of 4.8 nm diameter, protected with PET. Clusters with different ligands such as 4-FTP and BBS also show this behavior which suggests that the 'emergence of metallicity' is irrespective of the functionality of the thiol ligand.

## Introduction

The strong collective oscillations of electrons referred to as plasmon resonance[1] giving characteristic colors in optical absorption is the most fascinating property of noble metal nanoparticles[2-5] and this is the basis of most of their applications.[6-8] The occurrence of this collective phenomenon is attributed to the existence of metallicity[9] in such systems and is therefore important in the cluster size regime of metals. Investigation of the electronic structure by photoelectron spectroscopy has suggested the emergence of metallicity in the 200-400 atom window in several naked (ligand free) metal systems such as Hg, Cu and Au.[10-12] For several alkali metals like Na, K, Al, etc. the apperence of plasmon was studied extensively.[13-17]. Investigations of single particle conductivity by scanning electron spectroscopy and similar studies[18] have also proposed the emergence of metallicity in this window of size. On the other hand, large nanoparticles protected with monolayers of organic molecules, possessing metallicity in transport measurements[19] have been brought down to the cluster size regime by core etching protocols[20-22] wherein distinct luminescence in the visible region, characteristic of clusters has been observed.[23] Therefore, metallicity occurs beyond the regime of these clusters[24-31] but below the size regime of nanoparticles, in the range of silver nanoclusters. Thiolated gold clusters are normally more stable compared to silver clusters because Ag(0) is easily oxidisable in atmospheric conditions. Several gold clusters such as, $Au_{25}$,[32, 33] $Au_{28}$,[34] $Au_{36}$,[35] $Au_{38}$,[36] and $Au_{102}$[37] have been crystallized recently and many reports are there of their mass spectrometric assignments.[38, 39] Recently, Dass *et al*.[40] and Jin *et al*.[41] have shown the plasmonic feature in gold for ~ 76 kDa particles, protected with monolayers. In the case of silver, while clusters analogous to gold have not been made, there are reports of $Ag_{7,8}$,[22] $Ag_9$,[30] $Ag_{32}$,[27] and $Ag_{152}$[42] and a few others such as $Ag_{14}$,[43] $Ag_{16}$[44] and $Ag_{44}$[26, 31]; the latter ones have been crystallised.

In this paper, we report the emergence of plasmon-like optical absorption spectra in thiol protected silver clusters in solution which points to the appearance of metallicity in clusters composed of ~ 150 metal atoms. Our proposal of emergence of plasmon resonance is in accordance with studies so far[12] and point to similar results in other metal systems.[6-8]

## Experimental Section

### Materials

All the chemicals were commercially available and were used without further purification. Silver nitrate ($AgNO_3$, 99% Aldrich), silver trifluroacetate ($AgCOOCF_3$, 99%, Aldrich), sodium borohydride ($NaBH_4$, 99.9%, Aldrich), tetraoctylammoniuam

bromide (TOAB, 99%), 2-phenylethanethiol (PET, 98%, Aldrich); 4-(t-butyl)benzenethiol (BBS, 98%, Aldrich), 4-flurothio phenol (4-FTP, 98%, Aldrich) ethanol (Changshu Yangyuan Chemical, China, AR grade), acetonitrile, tetrahydrofuran, methanol and toluene (all are from Ranken, AR grade) were used in these synthesis.

**Synthesis of PET protected clusters**

The clusters protected with PET were prepared through the solid state method[22] and a solution phase synthetic route was followd for BBS protected clusters. They were synthesized by carefully controlling the conditions and were purified by solvent extraction protocols. These will be clearly understood in the light of the table given below which lists the synthetic details (Table 1). Initially, at room temperature (35-40 °C in Chennai, relative humidity-31%) X mg of $AgNO_3$ and Y µL of PETH were ground well in a clean agate mortar using a pestle. In some cases, tetraoctylammonium bromide (TOAB) was also used along with the ligand (details are mentioned in the table below). The color of the mixture changes to pale orange showing the formation of silver thiolate. To this mixture, Z mg of solid $NaBH_4$ was added and the content was mixed well. 5 mL of ethanol was added for washing the mixture. The mixture was kept for 15-30 s till there is a color change from pale orange to deep grey, which happened within 1 min. The contents were then taken in a centrifuge tube and centrifuged at 1600 rpm. The centrifugate was removed (except in the case of $Ag_{55}$ where ethanol was used as the extracting solvent) and the residue was dissolved in Q mL solvent (S). The clusters were obtained from the solvent extract, and were dark brown in color. Synthesis of ~$Ag_{530}$ took longer time and intially ~$Ag_{75}$ clusters were formed but after one day they got transformed to ~$Ag_{530}$ which is stable and TOAB facilitates the transformation.[45]

**Table 1.** Amounts of starting materials used for synthesizing various clusters.

| **Clusters** | **$AgNO_3$** (X/ mg) | **TOAB** (in mg) | **PETH** (Y/µL ) | **$NaBH_4$** (Z/mg) | **Solvent** (Q/mL) | **Yield** (%) | **Stability$^{\Phi}$** (day) |
|---|---|---|---|---|---|---|---|
| $Ag_{55}$ | 23 | 5 | 100 | 25 | Ethanol (5) | 64% | 3 |
| ~$Ag_{75}$ | 25 | --- | Glutathione* (12.5 mg) | Formic acid* (200 µL) | Water* | --- | 8 |
| ~$Ag_{114}$ | 23 | - | 100 | 25 | $CH_3CN$ (5) | 72% | 4 |
| $Ag_{152}$ | 23 | - | 100 | 25 | Toluene (5) | 82% | 10$^{\$}$ |
| ~$Ag_{423}$ | 23 | - | 100 | 25 | 50:50 mixture of Toluene/Methanol (5) | 64% | 5 |
| ~$Ag_{530}$ | 47 | 34 | 200 | 30 | Toluene (20 ) | 76% | 14$^{\#}$ |
| Ag NP | 47 | - | 100 | 30 | Toluene (5) | 84% | 30 |

*, # and $ refer to the coresponding references given below and ϕ refers to stability in the ambient laboratory conditions.

* Reference[46]

$ Reference[42]

[#] Reference[45]

**Synthesis of BBS protected cluster**

20 mg of $AgNO_3$ was dissolved in 3 mL of methanol. 3 mL of toluene was also added to the solution. Then BBS (1:6 mole ratios with respect to silver) was added to it, under stirring. It formed an Ag-thiolate complex. During this process, the color of the solution changes from deep yellow to light yellow. After 30 min, 2 mL fresh ice cold solution of $NaBH_4$ (1:10 mole ratios with respect to silver) was added. The yellow color changes to dark brown. Stirring was continued for 30 minutes. Two separate layers were observed. Top layer contains the cluster which was taken out and characterized further.

**Synthesis of $Ag_{44}$ cluster**

$Ag_{44}$ cluster was synthesised using a reported procedure.[28]

**Instrumentation**

UV/Vis spectra were measured with a Perkin Elmer Lambda 25 instrument in the range of 200 - 1100 nm. The spectra were corrected by Jacobian factor (see below). High resolution transmission electron microscopy of clusters was carried out with a JEOL 3010 instrument with a UHR polepiece. The samples were drop cast on carbon-coated copper grids and allowed to dry under ambient conditions. Matrix-assisted desorption ionization mass spectrometry (MALDI MS) studies were conducted using a Voyager-DE PRO Bio-spectrometry Workstation of Applied Bio-systems. A pulsed nitrogen laser of 337 nm was used for the MALDI MS studies. Mass spectra were collected in positive ion mode and were averaged for 200 shots. For sample preparation, the as-synthesized clusters were mixed with DCTB (*trans*-2-[3-(4-*t*-butylphenyl)-2-methyl-2-propenylidene]malononitrile) matrix (12.5 mg/ml in tolune) in 1:1 and 2:1 volume ratios, followed by immediate spotting on the MALDI plate. Scanning electron microscopy (SEM) and energy dispersive X-ray (EDAX) measurements were performed with a FEI QUANTA-200 SEM. For measurements, samples were drop cast on an indium tin oxide (ITO) coated glass as well as on carbon tape and subsequently dried under vacuum. DLS was done with a Horiba instrument. X-ray photoelectron spectroscopy (XPS) measurements were conducted using an Omicron ESCA Probe spectrometer with polychromatic MgKα X-rays (hυ=1253.6 eV). The samples were spotted as drop-cast films on a sample stub. Constant analyzer energy of 20 eV was used for the measurements.

**Results and Discussion**

The core size of each cluster sample was characterized (Fig. 1) by matrix assisted laser desorption ionization mass spectrometry (MALDI MS) with DCTB as the matrix which is effective for organic soluble clusters.[42, 46-48] The spectra show the existence of eight distinctly different clusters with characteristic peaks at 10.3, 13.7, 18.6, 24.5, 33.4, 60 k and 70.9 k. Assuming the ions to be monocationic, as suggested by their peak width, the clusters responsible for these peaks are assigned to be $Ag_{55}(PET)_{31}$, $\sim Ag_{75}(PET)_{40}$,[46] $\sim Ag_{114}(PET)_{46}$, $Ag_{152}(PET)_{60}$,[42] $\sim Ag_{202}(BBS)_{70}$, $\sim Ag_{423}(PET)_{105}$, and $\sim Ag_{530}(PET)_{100}$,[45] respectively (as peaks are ill-defined in a few cases, the composition is indicated with a '~' symbol, as practiced by others[49]). Compositions suggsted here have been supported by elemental analysis and XPS as well (see below). In most of the cases (labeled as 'a', 'b', 'c', 'd' in Fig. 1), the spectra correspond to sharp and single features. This is especially noticeable in 'a' and 'd' corresponding to $Ag_{55}$ and $Ag_{152}$. For 'b', there is a weak feture at the high mass side and for 'c', there is a weak shoulder at the high mass side. Due to these reasons, we suggest only approximate compositions for them. Detailed characterization of each cluster is beyond the scope of this work, and some of the clusters ($Ag_{44}$, $\sim Ag_{75}$, $Ag_{152}$ and $\sim Ag_{530}$) have been described previously.[26, 28, 31, 42, 45, 46] It is important to note that the spectra were collected at the threshold laser powers (fluences) where observable fragmentation is not seen. Above a characteristic laser power, fragmentation was seen, normally due to the loss of the monolayer, AgSR, $Ag(SR)_2$ or R.[42, 46] Such systematic losses and fragmentation arising from cleavages in $Ag_n$-S-R are well known upon UV laser irradiation and such processes have been useful in understanding the core sizes.[50] For example, in the case of $Ag_{152}PET_{60}$, where we could see a gradual fragmentation with increase in laser power (Fig. S1, ESI†) and after a certain laser power, no further fragmentation was observed. The spectra are also composed of a few other clusters of higher masses (traces 'e', 'f' and 'g') which exhibit multiple features. Specific clusters have not been obtained in such cases so far.

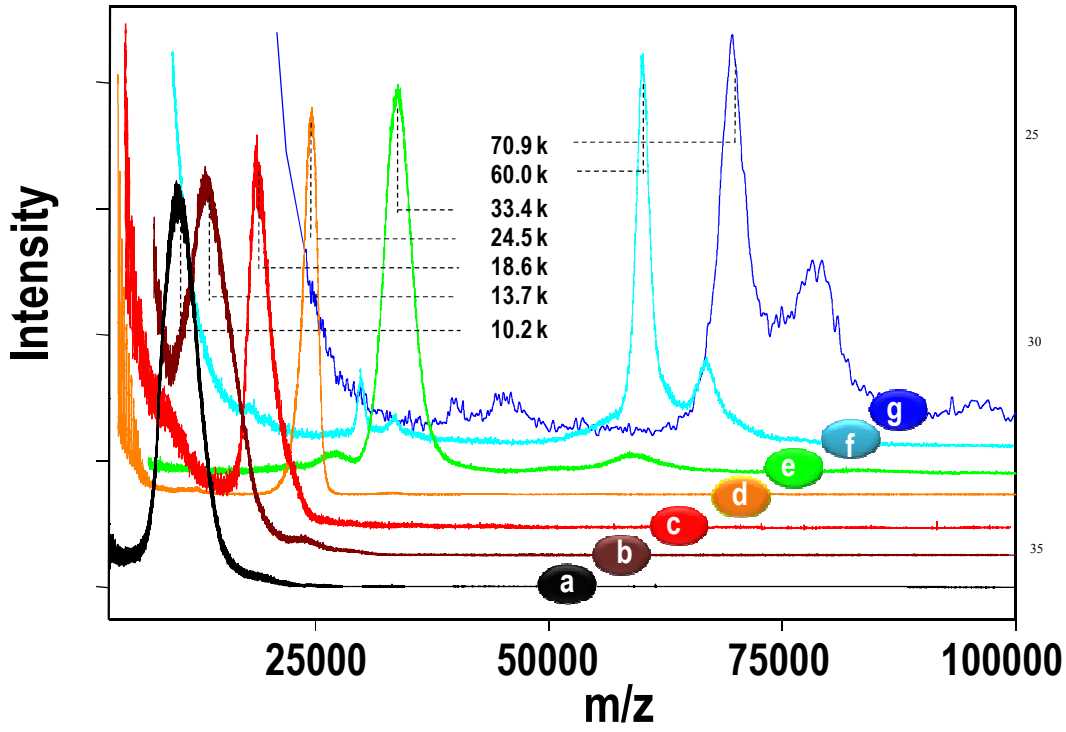


Fig. 1. *MALDI MS spectra (collected in positive mode) of silver clusters prepared in solution. All the clusters were purified through solvent extraction before spotting for MALDI MS studies. Threshold laser fluence was used throughout the experiment to avoid fragmentation. The spectra show a series of clusters with peak maxima ranging from 10.2 to 70.9 k. Almost all of them (except 'f' and 'g' which have some other features with reduced intensity) show sharp single features which confirm the formation of one dominant cluster in each case. The FWHM varied from 1.5 to 5 kDa. The peaks (from bottom to top) were assigned as:* $Ag_{55}(PET)_{31}$ *[a],* $\sim Ag_{75}(PET)_{40}$ *[b],* $\sim Ag_{114}(PET)_{46}$ *[c],* $Ag_{152}(PET)_{60}$ *[d],* $\sim Ag_{202}(BBS)_{70}$ *[e],* $\sim Ag_{423}(PET)_{105}$ *[f], and* $\sim Ag_{530}(PET)_{100}$ *[g]. Spectra have been shifted vertically for clarity.*

Even in those cases, however, the spectra are dominated by one major feature with a few other clusters existing with reduced intensity. Another interesting feature was the full width at half maximum (FWHM ) of each spectrum. It varied from 1.5 to 5 k. In a, c, d and f, the peak the peak width is very small (below 3 k), this is not seen in any of silver clusters reported so far.

It is important to note here that all the peaks are indeed broad in comparison to molecules of similar masses, such as smaller proteins. However, we must note that the peak is sharper than protein protected silver, gold and silver-gold alloy clusters, which are similar to those considered here.[51-53] In Fig. S2A, ESI†, we have plotted the MALDI MS spectra of $Ag_{152}$ cluster (of the most narrower width), a small protein, lysozyme in its native state and that of lysozyme–gold cluster (all in linear positive ion mode). We see that while the native protein spectrum is sharper ($\Delta m$=0.3 Da), the mass feature of the protein cluster is broader ($\Delta m$=2.5 Da) and the width is comparable to that of the silver cluster. This broadening of the protein-gold cluster is due to changes in the native structure of the protein upon cluster formation. It may also be noted that the protein protected clusters shown are those of Au, which has only one isotope. In the case of silver, there is a natural isotope width and this spread is large in the case of a multi-atom cluster (see below). The data suggest that the inherent width in silver clusters is comparable to molecular systems of similar masses. For comparision, MALDI MS of $Ag_{152}$ cluster was plotted along with the well-chracterised $Ag_{44}$ cluster (Fig. S3, ESI†). The data suggest that spectra of silver clusters are indeed broad in nature, even if they are atomically precise.

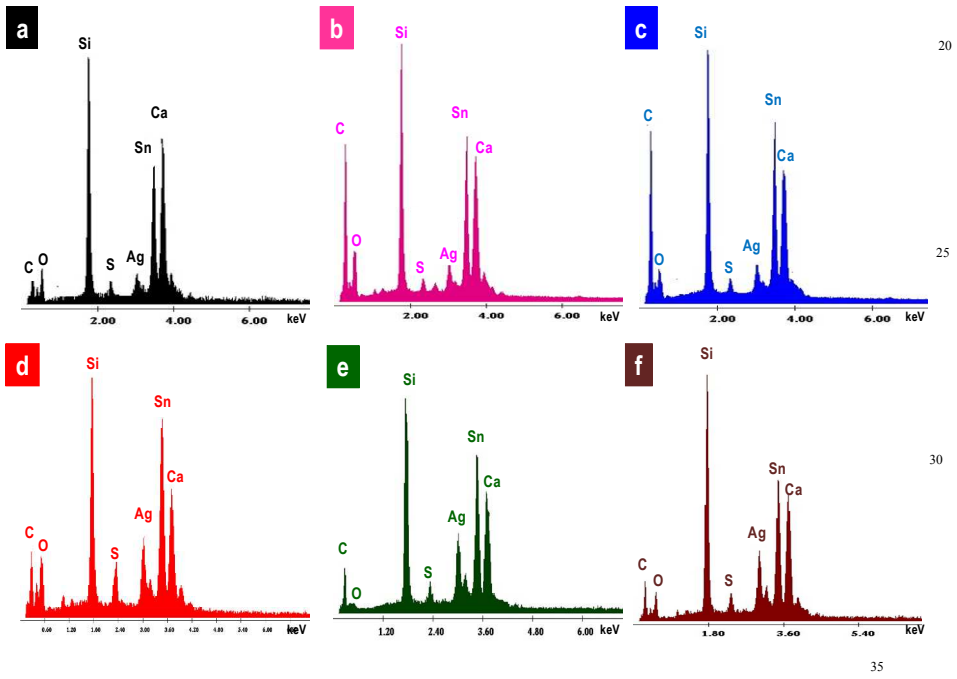


*Fig. 2. SEM/EDAX of $Ag_{55}$ (a), ~$Ag_{75}$ (b), ~$Ag_{114}$ (c), $Ag_{152}$ (d), ~$Ag_{423}$ (e) and ~$Ag_{530}$ (f). Expected elements are seen. The spectra were colected from a drop cast sample on an ITO plate. Peaks coresponding to Si, Sn, Ca and O are from the substrate.*

Electrospray ionization (ESI) is a preferred method in several thiolated clusters. However, for silver clusters, ESI MS is still not ideal as intact ionization is difficult. More ESI MS data are available for gold clusters; however, it is important to note that gold has only one isotope while silver has two at m/z 107 and m/z 109 with 50:50 intensity. This adds additional width to the mass feature of silver clusters. Besides, silver-sulfur binding is weaker which makes the intact cluster less stable and ligand losses occur upon ionization. Both these contribute to the increased width of the mass spectrum of silver clusters (in comparison to gold). In the case of $Au_{25}PET_{18}$, the spectrum (Fig. S2B, ESI†) is measurable with improved resolution in the reflectron mode. As typical reflectron measurements are limited to m/z 10,000, the present silver clusters at m/z > 10,000 could not yield better peak shapes in such measurements.

The SEM/EDAX data further support the composition of the clusters. Fig. 2 shows the corresponding EDAX spectra of $Ag_{55}$ (a), ~$Ag_{75}$ (b), ~$Ag_{114}$ (c), $Ag_{152}$ (d), ~$Ag_{423}$ (e) and ~ $Ag_{530}$ (f). Here clusters were drop cast on indium tin oxide (ITO) coated glass plates. The spectrum of ~$Ag_{202}$ was collected from a drop cast sample (on a carbon tape) and is given in Fig. S4, ESI†. Expected elements are seen in each case and the Ag:S ratios were 1:0.60, 1: 0.58, 1: 0.39, 1: 0.43, 1: 0.40, 1: 0.34 and 1: 0.37 for $Ag_{55}$, ~$Ag_{75}$, ~$Ag_{114}$, $Ag_{152}$, ~$Ag_{202}$, ~$Ag_{423}$ and ~$Ag_{530}$, respectively whereas the expected ratios are 1:0.56, 1:0.53, 1:0.36, 1:0.39, 1:0.34, 1:0.25 and 1:0.18. For the last two cases, there is excess amount of thiol in the sample, which is probably needed for cluster stabilisation.[42] As ~$Ag_{423}$ and ~$Ag_{530}$ samples are not pure, as seen from their mass spectra, their atomic ratios deviate significantly from the expected ones.

These clusters with precise core sizes are observable in TEM, where well defined cores ranging from 1.12 nm to 4.0 nm are observed (Fig. 3 and Fig. S5, ESI†). The particle size increases with the nuclearity of the cluster. The size distribution shown in the insets of each of these images (Fig. 3) confirmed that the synthetic protocol yielded the desired results. A narrow size distribution suggests the monodispersity of the as-syntheised clusters. The average core diameters were 1.12, 1.32, 1.75, 2.0,

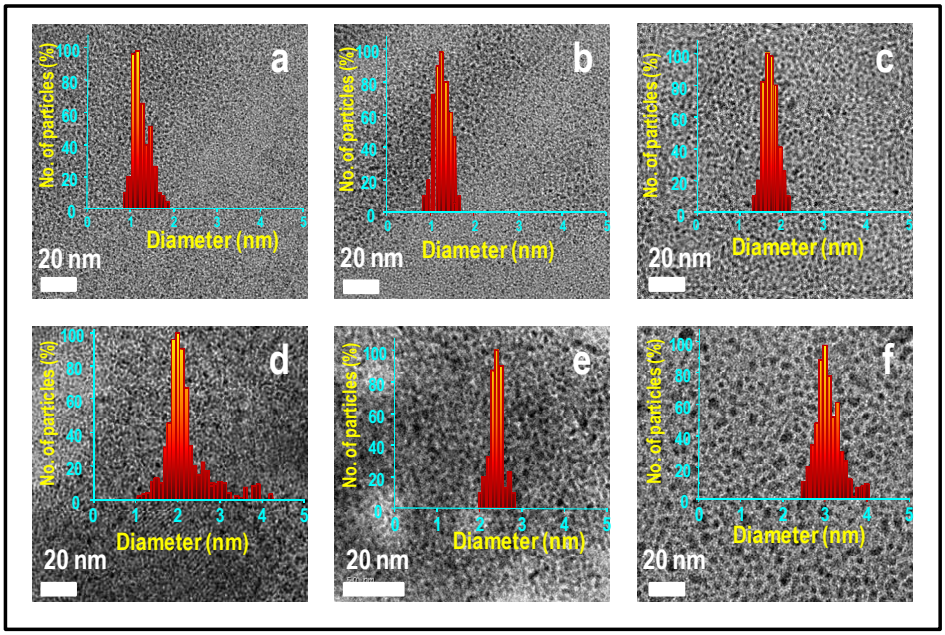


*Fig. 3. HRTEM images of clusters: $Ag_{55}$ [a], ~$Ag_{75}$ [b], ~$Ag_{114}$ [c], $Ag_{152}$ [d], ~$Ag_{202}$ [e] and ~$Ag_{423}$ [f]. The images show a gradual increase in cluster size from left to right ('a' to 'c' and 'd' to 'f'). Inset of all images show the size distribution of clusters, which varies from 1.12 to 3.20 nm. Some bigger nanoparticles were also seen which could be due to aggregation upon electron beam irradiation.*

2.61 and 3.20 nm for $Ag_{55}$, ~$Ag_{75}$, ~$Ag_{114}$, $Ag_{152}$, ~$Ag_{202}$ and ~$Ag_{423}$, respectively. Polydispersity is seen in image 'f', in agreement with the mass spectrum (Fig. 1f). The cluster ~$Ag_{530}$ is about 3.61 nm in diameter (Fig. S5, ESI†) which also shows polydispersity. To further support the monodispersity, dynamic light scatering mesuements were carried out for the PET protected clusters (Fig. S6, ESI†) which also shows a narrow size dustribution for smaller clusters up to $Ag_{152}$. For ~$Ag_{423}$, the peak become broader as expected from MALDI MS data which suggests the existence of other species in minor proportions.

As such clusters are prone to electron beam induced damage[21] and subsequent core size evolution with increasing electron beam irradiation, a few aggregates and cores of larger sizes are observed in the images. For comparison, TEM images of Ag@PET nanoparticle is given in supporting information (Fig. S7, ESI†). It has a wide range of sizes starting from 3 to 8 nm with an avarage diameter of 4.8 nm.

The optical absorption spectra of clusters of smaller sizes show multiple features corresponding to the distinct transitions between the discrete energy states (Fig. 4 and Fig. S8, ESI†). In the still smaller regime of $Ag_7$,[22] $Ag_8$ and $Ag_9$[30], $Ag_{14}$,[43] $Ag_{16}$,[44] $Ag_{32}$,[27], $Ag_{44}$,[28] etc. many more features are observed. In the case of $Ag_7$, two humps corresponding to 550 and 600 nm were seen.[22] Similarly for $Ag_9$, four features at 450, 489, 629 and 886 nm were observed.[30] Multiple feature was also seen from the cluster reported by Kitaev.[24] In the magic numbered glutathione protected silver clusters,[29] in the bands 2, 6, 9 and 13 separated by polyacryl amide gel electrophoresis (PAGE), distinct optical features are seen. Multiple step-like fetures were seen in the absence of plasmon in their optical spectrum. Recently, from Bigoni's group, $Ag_{32}$ was identified by mass spectrometry[27] where also we see the same step-like features along with the absence of plasmon-like absorption which comes around 390-430 nm region for water-soluble clusters. Similar is the case for $Ag_{44}$ cluster reported by Dass *et al.*[28] Surprisingly, compared to other silver clusters, this system shows five pronounced and three weak bands it its optical spectrum.

From the data presented in Fig. 4, we see that as the sizes increase, these low energy features disappear and a large oscillator strength is accumulated around 450 nm. Smaller clusters show molecule- like properties with discreate energy levels which are reflected in their optical spectra. $Ag_{44}$ cluster shows five itense bands along with three weak bands similar to

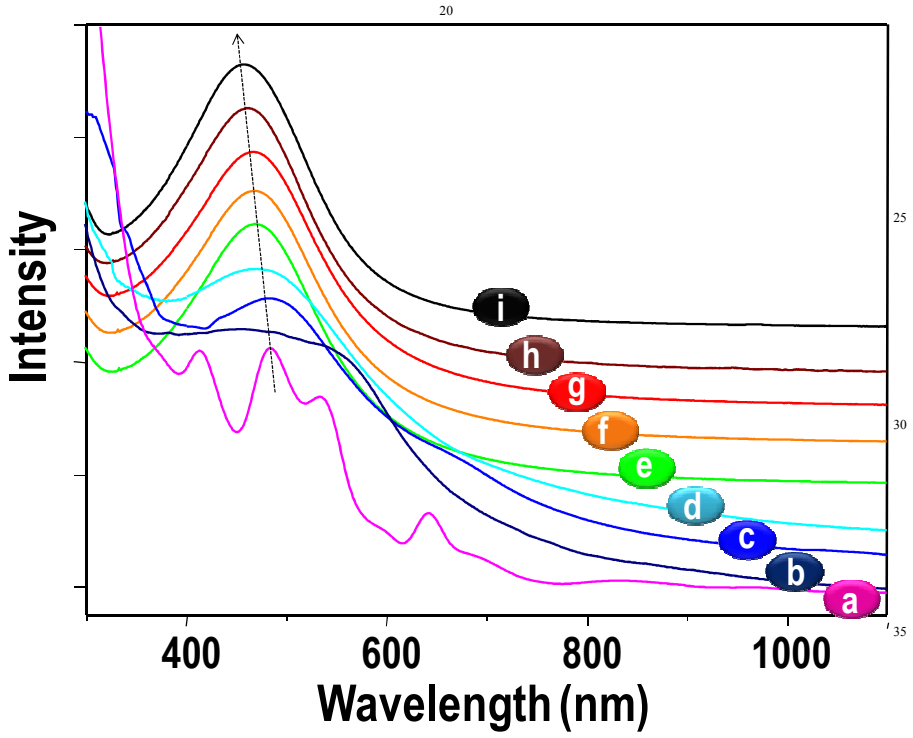


*Fig. 4. UV/Vis spectra of clusters with wavelength on the x-axis. From bottom to up: $Ag_{44}$ [a], $Ag_{55}$ [b], ~$Ag_{75}$ [c], ~$Ag_{114}$ [d], $Ag_{152}$ [e], ~$Ag_{202}$ [f], ~$Ag_{423}$ [g], ~$Ag_{530}$ [h] and AgNPs [i]. Spectra have been shifted vertically for clarity. The spectra show multiple features up to 'd' (namely, eight bands for $Ag_{44}$, two energy bands for $Ag_{55}$ and ~$Ag_{114}$, and three for ~$Ag_{75}$). But from 'h' to 'i', only a single plasmon-like feature was observed with a small blue shift (i. e. at higher energy).*

that reported by Harkness *et al.*[28] For $Ag_{55}$, two distinct features at 450 (2.75) and 550 (2.25) nm (eV) are seen along with a hump at 495 (2.50) nm (eV). In $Ag_{75}$, the features appear at 475 (2.61 ) and 630 (1.96) nm (eV) along with a shoulder at 430 (2.88) nm (eV). ~$Ag_{114}$ shows two features at 464 (2.67 ) and 540 (2.29 ) nm (eV). $Ag_{152}$, ~$Ag_{202}$, ~$Ag_{423}$, ~$Ag_{530}$ and AgNP show a single peak at 462 (2.68), 460 (2.69 ), 458 (2.70 ), 457 (2.71 ) and 454 (2.73) nm (eV), respectively. Merging of features occurs around $Ag_{152}$. All the smaller clusters also show significant absorption in the 3-4 eV (413-310 nm) window, possibly arising from the Ag-thiolate shell protecting the metal core. Note that Ag-SR thiolate in toluene solutions typically show absorption in the ultraviolet. At $Ag_{152}$ and beyond, only one feature is seen. Beyond this, the peak position shifts only marginally upon increase in cluster size from ~$Ag_{202}$ to ~$Ag_{530}$. As larger clusters, such as ~$Ag_{202}$ and beyond are not pure, their spectra may have contributions from impurity particles as well. However, from $Ag_{152}$ itself, which is atomically precise, the spectra resemble that of Ag nanoparticles protected with PET, whose peak maximum occurs 462 nm (Fig. S8, ESI†). For water soluble nanoparticles, SPR occurs in the 390-440 nm window, depending on size. Part of the reason for a red-shifted peak in PET protected particles is the organic shell and the other reason is the medium surrounding the particles. Surface plasmon resonance is greatly influenced by the dielectric constant of the solvent. In this case, the solvents are organic which have much lesser dielectric constants (toluene = 2.4 at 20 °C) than water (80.4 at 20 °C). This could be the reason for plasmon shift of organic soluble nanoparticles, as suggested by Mie theory.[1, 2] The spectra as a function of energy are plotted in Fig. S8, ESI†. For more clarity, peak position is plotted against reciprocal of diameter (Fig. 5a). The average diameter was taken from the TEM analysis. It shows an almost linear behavior, in agreement with the spherical shell model.[54-56] Optical absorption spectra of smaller clusters for both gold and silver

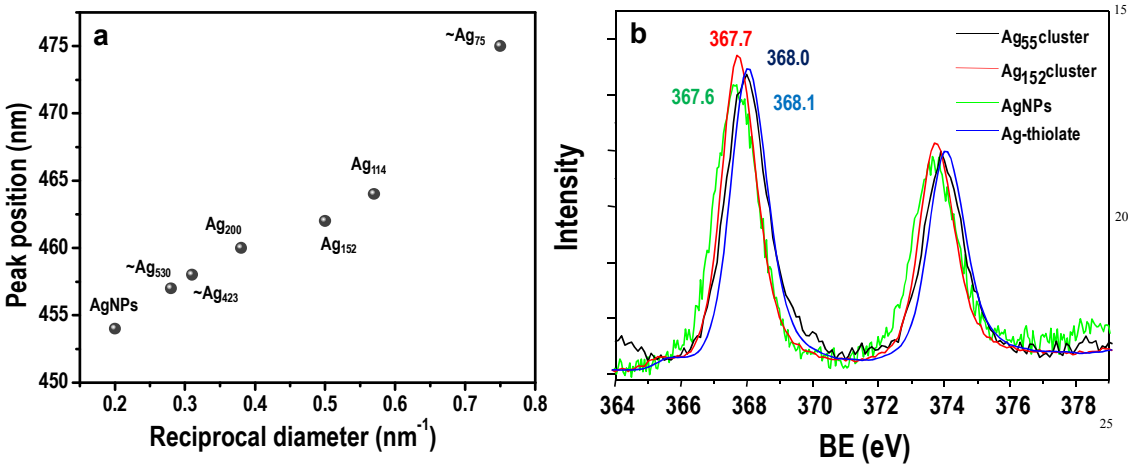


*Fig. 5. A plot of absorption peak positions with respect to reciprocal of cluster diameter (a). The average core diameter was taken from the TEM size distribution. Expanded XPS of the Ag3d region of $Ag_{55}$, $Ag_{152}$, AgNPs and Ag(I)-thiolate (b).*

exhibit multiple features. As the size decreases below 55 as in the case of $Ag_{44}$, $Ag_{32}$, $Ag_9$, etc.[27, 28, 30, 31] many more features appear in the spectra, especially in the red region. Many of these transitions have large contributions from the thiolate shell as shown by time-dependent density functional theory (TDDFT) calculations.[57, 58] A comparison of the calculated optical spectrum of various clusters, suggest a systematic trend for the core-derived transitions.[57, 58] In the limit of large cluster sizes, this transitions converge to the plasmon resonance. From a simplistic argument, one can see that as the proportion of ligand derived states decrease, the dipole transition of the core will be dominant in the optical absorption spectra. Comparing the spectra of the clusters listed here, it is seen that large optical density, similar to plasmon resonance, appears in the vicinity of $Ag_{152}$. This cluster is expected to have 92 free electrons, whereas metallicity is suggsetd to occur around 60 atoms, in the case of naked gas phase clusters.[12] However, the thiolated cluster systems are not identical to the bulk *fcc* solid. For some well characterized clusters of the type $Ag_{44}$, the cage is understood to be a Keplerate solid.[26, 31] This hollow cage structure is distinctly different from the molecular analogues of the bulk metal which can result in a variation of the optical absorption spectrum.

Ultraviolet photoelectron spectroscopic studies of these clusters were attempted but nothing significant came out from this study. X-ray photoelectron spectroscopy gives some good information about the valence state of silver. XPS was also used n evaluating elemental composition of the samples, although these data are not presented here. For consistency in analysis, we have collected the XPS of four consecutive systems which are $Ag_{55}$, $Ag_{152}$, AgNPs and Ag(I)-thiolate (Fig. 5b). The $Ag_{55}$ cluster shows the $3d_{5/2}$ peak at 368.0 eV which is near to the Ag-thiolate peak (368.1 eV). This could be because more number of Ag(I) is present compared to Ag(0). On the other hand, $Ag_{152}$ cluster shows the peak at 367.7 eV which is closer to the AgNPs, further suggesting a change in the properties of materials in the $Ag_{152}$ regime.

There have been several photoelectron spectroscopic investigations on the emergence of metallicity in metal clusters.[10, 12, 59] These are generally discussed in the light of initial and final state effects.[60] Electronic relaxation of the final state and electronic interaction with the support contributing to the additional screening are important in determining the final state effect. Intrinsic electronic structure stabilizing the cluster contributes to the initial state effect.[60] While systematic energy shifts of the 4f binding energy is observed in supported gold clusters, no such effect is seen in supported silver clusters.[60] The change in ionization energy as well as the increase width of the photoelectron spectra are proportional to 1/R as suggested by spherical shell model.[54-56] Electronic and geometric effects contribute to changes in the behavior. In the case of supported Ag clusters, no binding energy shift was observed; this may be attributed to the large separation of the 4d and 5s orbitals in comparison to gold, due to the lack of relativistic contraction for silver.[60] As a consequence, no large redistribution occurs between

the s and d orbitals. While this is the case of un-passivated clusters, in the data presented in Fig. 5b we see a small shift to the increased binding energy in clusters and thiolate in comparison to the nanoparticles. This attributed to the large proportion of $Ag^+$. However, when it comes to $Ag_{152}$, the spectrum is almost identical to that of AgNPs. Thus while photoemission using core level is important to distinguish the clusters from bulk for gold, no large difference are seen for silver.[60] The data are consistent for the monolayer protected and naked clusters as shown here.

The present results suggest the emergence of plasmon-like optical absorption around $Ag_{152}$. In silver clusters, metallicity is seen around 60 atoms in photoelectron spectroscopic studies, as mentioned before.[12] Unlike in the case of naked clusters which was used for photoelectron spectroscopy, the clusters used here are monolayer protected which have distinct cores of smaller dimension. Cluster with a different ligand (BBS) also shows the plasmonic feature which confirms the fact that emergence of metallicity is the inherent property of the metal. The origin of metallicity is suggested to be around $Ag_{152}$ which has a core of 92 atoms and a shell composed of $Ag_{60}SR_{60}$.[42]

## Conclusions

In summary, we report the occurrence of plasmon-like optical absorption feature in silver clusters prepared in solution. A range of clusters with varying nuclearities were synthesised and analysed through MALDI MS. Well-defined TEM with gradual increase in size was observed. Different ligands were used to understand the silver-thiolate binding chemistry and its influence on the appearance of plasmon. Based on the emergence of collective electron resonance in the 150 atom-regime, we suggest that this is the window where metallicity originates for silver, in monolayer protected clusters.

## Acknowledgments

We thank the Department of Science and Technology, Government of India for constantly supporting our research program on nanomaterials. I. C. Thanks IITM for research fellowship.

## Notes and references

**DST Unit of Nanoscience (DST UNS) and Thematic Unit of Excellence (TUE), Department of Chemistry, Indian Institute of Technology Madras, Chennai 600 036, India; Fax: 91-44-2257 0545; E-mail: pradeep@iitm.ac.in*

*†Electronic Supplementary Information (ESI) available: [details of Laser dependent fragmentation, SEM-EDAX of ~$Ag_{202}$, TEM of ~$Ag_{530}$ and nanoparticles and corresponding energy-dependent UV/Vis spectra, DLS, and comparative MALDI MS .]. See DOI: 10.1039/b000000x/*

1. G. Mie, *Annalen der Physik*, 1908, **330**, 377-445.
2. C. Burda, X. Chen, R. Narayanan and M. A. El-Sayed, *Chemical Reviews*, 2005, **105**, 1025-1102.
3. J. Turkevich, P. C. Stevenson and J. Hillier, *Discussions of the Faraday Society*, 1951, **11**, 55-75.
4. M. Brust, M. Walker, D. Bethell, D. J. Schiffrin and R. Whyman, *Journal of the Chemical Society, Chemical Communications*, 1994, 801-802.
5. P. V. Kamat, *The Journal of Physical Chemistry B*, 2002, **106**, 7729-7744.
6. I. Chakraborty, T. Udayabhaskararao and T. Pradeep, *Journal of hazardous materials*, 2012, **211**, 396-403.
7. I. Chakraborty, U. B. R. Thumu, G. K. Deepesh and T. Pradeep, *Journal of Materials Chemistry B*, 2013,1, 4059-4064.
8. A. George, E. S. Shibu, S. M. Maliyekkal, M. S. Bootharaju and T. Pradeep, *ACS Applied Materials & Interfaces*, 2012, **4**, 639-644.
9. M. T. Murphy, S. J. Curran, J. K. Webb, H. Menager and B. J. Zych, *Mon. Not. R. Astron. Soc.*, 2007, **376**, 673-681.
10. O. Cheshnovsky, K. J. Taylor, J. Conceicao and R. E. Smalley, *Physical Review Letters*, 1990, **64**, 1785-1788.
11. B. v. Issendorff and O. Cheshnovsky, *Annual Review of Physical Chemistry*, 2005, **56**, 549-580.
12. K. J. Taylor, C. L. Pettiette-Hall, O. Cheshnovsky and R. E. Smalley, *J. Chem. Phys.*, 1992, **96**, 3319-3329.
13. T. Andersson, C. Zhang, A. Rosso, I. Bradeanu, S. Legendre, S. E. Canton, M. Tchaplyguine, G. Ohrwall, S. L. Sorensen, S. Svensson, N. Martensson and O. Bjorneholm, *The Journal of Chemical Physics*, 2011, **134**, 094511-094516.
14. T. Andersson, C. Zhang, M. Tchaplyguine, S. Svensson, N. Martensson and O. Bjorneholm, *The Journal of Chemical Physics*, 2012, **136**, 204504-204505.
15. V. B. Gildenburg, V. A. Kostin and I. A. Pavlichenko, *Physics of Plasmas*, 2011, **18**, 092101-092106.
16. K. Höflich, U. Gösele and S. Christiansen, *Physical Review Letters*, 2009, **103**, 087404.
17. V. Senz, T. Fischer, P. Oelßner, J. Tiggesbäumker, J. Stanzel, C. Bostedt, H. Thomas, M. Schöffler, L. Foucar, M. Martins, J. Neville, M. Neeb, T. Möller, W. Wurth, E. Rühl, R. Dörner, H. Schmidt-Böcking, W. Eberhardt, G. Ganteför, R. Treusch, P. Radcliffe and K. H. Meiwes-Broer, *Physical Review Letters*, 2009, **102**, 138303.
18. L. F. Chi, M. Hartig, T. Drechsler, T. Schwaack, C. Seidel, H. Fuchs and G. Schmid, *Appl. Phys. A: Mater. Sci. Process.*, 1998, **66**, S187-S190.
19. H. Moreira, J. Grisolia, N. M. Sangeetha, N. Decorde, C. Farcau, B. Viallet, K. Chen, G. Viau and L. Ressier, *Nanotechnology*, 2013, **24**, 095701.
20. Y. Shichibu, Y. Negishi, H. Tsunoyama, M. Kanehara, T. Teranishi and T. Tsukuda, *Small*, 2007, **3**, 835-839.
21. L. Dhanalakshmi, T. Udayabhaskararao and T. Pradeep, *Chemical Communications*, 2012, **48**, 859-861.
22. T. Udaya Bhaskara Rao and T. Pradeep, *Angewandte Chemie International Edition*, 2010, **49**, 3925-3929.
23. E. S. Shibu, M. A. H. Muhammed, T. Tsukuda and T. Pradeep, *The Journal of Physical Chemistry C*, 2008, **112**, 12168-12176.
24. N. Cathcart and V. Kitaev, *The Journal of Physical Chemistry C*, 2010, **114**, 16010-16017.
25. I. Chakraborty, W. Kurashige, K. Kanehira, L. Gell, H. Häkkinen, Y. Negishi and T. Pradeep, *The Journal of Physical Chemistry Letters*, 2013, 3351-3355.
26. A. Desireddy, B. E. Conn, J. Guo, B. Yoon, R. N. Barnett, B. M. Monahan, K. Kirschbaum, W. P. Griffith, R. L. Whetten, U. Landman and T. P. Bigioni, *Nature*, 2013, **501**, 399-402.
27. J. Guo, S. Kumar, M. Bolan, A. Desireddy, T. P. Bigioni and W. P. Griffith, *Analytical Chemistry*, 2012, **84**, 5304-5308.

28. K. M. Harkness, Y. Tang, A. Dass, J. Pan, N. Kothalawala, V. J. Reddy, D. E. Cliffel, B. Demeler, F. Stellacci, O. M. Bakr and J. A. McLean, *Nanoscale*, 2012, **4**, 4269-4274.
29. S. Kumar, M. D. Bolan and T. P. Bigioni, *Journal of the American Chemical Society*, 2010, **132**, 13141-13143.
30. T. U. B. Rao, B. Nataraju and T. Pradeep, *Journal of the American Chemical Society*, 2010, **132**, 16304-16307.
31. H. Yang, Y. Wang, H. Huang, L. Gell, L. Lehtovaara, S. Malola, H. Häkkinen and N. Zheng, *Nat Commun*, 2013, **4**.
32. M. W. Heaven, A. Dass, P. S. White, K. M. Holt and R. W. Murray, *Journal of the American Chemical Society*, 2008, **130**, 3754-3755.
33. M. Zhu, C. M. Aikens, F. J. Hollander, G. C. Schatz and R. Jin, *Journal of the American Chemical Society*, 2008, **130**, 5883-5885.
34. C. Zeng, T. Li, A. Das, N. L. Rosi and R. Jin, *Journal of the American Chemical Society*, 2013, **135**, 10011-10013.
35. C. Zeng, H. Qian, T. Li, G. Li, N. L. Rosi, B. Yoon, R. N. Barnett, R. L. Whetten, U. Landman and R. Jin, *Angewandte Chemie International Edition*, 2012, **51**, 13114-13118.
36. H. Qian, W. T. Eckenhoff, Y. Zhu, T. Pintauer and R. Jin, *Journal of the American Chemical Society*, 2010, **132**, 8280-8281.
37. P. D. Jadzinsky, G. Calero, C. J. Ackerson, D. A. Bushnell and R. D. Kornberg, *Science*, 2007, **318**, 430-433.
38. A. Dass, *J Am Chem Soc*, 2009, **131**, 11666-11667.
39. P. R. Nimmala, B. Yoon, R. L. Whetten, U. Landman and A. Dass, *The journal of physical chemistry. A*, 2013, **117**, 504-517.
40. A. Dass, *Journal of the American Chemical Society*, 2011, **133**, 19259-19261.
41. H. Qian, Y. Zhu and R. Jin, *Proceedings of the National Academy of Sciences*, 2012.
42. I. Chakraborty, A. Govindarajan, J. Erusappan, A. Ghosh, T. Pradeep, B. Yoon, R. L. Whetten and U. Landman, *Nano Letters*, 2012, **12**, 5861-5866.
43. H. Yang, J. Lei, B. Wu, Y. Wang, M. Zhou, A. Xia, L. Zheng and N. Zheng, *Chemical Communications*, 2013, **49**, 300-302.
44. H. Yang, Y. Wang and N. Zheng, *Nanoscale*, 2013, **5**, 2674-2677.
45. K. S. Sugi, I. Chakraborty, T. Udayabhaskararao, J. S. Mohanty and T. Pradeep, *Particle & Particle Systems Characterization*, 2013, **30**, 241-243.
46. I. Chakraborty, T. Udayabhaskararao and T. Pradeep, *Chemical Communications*, 2012, **48**, 6788-6790.
47. S. Knoppe, A. C. Dharmaratne, E. Schreiner, A. Dass and T. Bulˆrgi, *Journal of the American Chemical Society*, 2010, **132**, 16783-16789.
48. A. Dass, A. Stevenson, G. R. Dubay, J. B. Tracy and R. W. Murray, *Journal of the American Chemical Society*, 2008, **130**, 5940-5946.
49. Y. Negishi, R. Arai, Y. Niihori and T. Tsukuda, *Chemical Communications*, 2011, **47**, 5693-5695.
50. Y. Negishi, C. Sakamoto, T. Ohyama and T. Tsukuda, *The Journal of Physical Chemistry Letters*, 2012, **3**, 1624-1628.
51. K. Chaudhari, P. L. Xavier and T. Pradeep, *ACS Nano*, 2011, **5**, 8816-8827.
52. A. Mathew, P. R. Sajanlal and T. Pradeep, *Journal of Materials Chemistry*, 2011, **21**, 11205-11212.
53. J. S. Mohanty, P. L. Xavier, K. Chaudhari, M. S. Bootharaju, N. Goswami, S. K. Pal and T. Pradeep, *Nanoscale*, 2012, **4**, 4255-4262.
54. R. B. Wyrwas, M. M. Alvarez, J. T. Khoury, R. C. Price, T. G. Schaaff and R. L. Whetten, *Eur. Phys. J. D*, 2007, **43**, 91-95.
55. O. Varnavski, G. Ramakrishna, J. Kim, D. Lee and T. Goodson, *Journal of the American Chemical Society*, 2009, **132**, 16-17.
56. W. A. de Heer, *Reviews of Modern Physics*, 1993, **65**, 611-676.
57. H. Hakkinen, *Chemical Society Reviews*, 2008, **37**, 1847-1859.
58. H. Hakkinen, *Nat Chem*, 2012, **4**, 443-455.
59. I. B. von and O. Cheshnovsky, *Annu. Rev. Phys. Chem.*, 2005, **56**, 549-580.
60. S. Peters, S. Peredkov, M. Neeb, W. Eberhardt and M. Al-Hada, *Surface Science*, 2013, **608**, 129-134.